Jpn. J. Appl. Phys. Vol. 31 (1992) pp. 3779-3785
Part 1, No. 12A, December 1992

Numerically Simulated and Experimentally Obtained X-Ray Section Topographs of a Spherical Strain Field in a Floating Zone Silicon Crystal

Kouhei OKITSU, Satoshi IIDA, Yoshimitsu SUGITA, Hiroshi TAKENO*, Yasuyoshi YAGOU** and Hiroshi KAWATA[1]

Department of Physics, Toyama University, Toyama 930
[1]*National Laboratory for High Energy Physics, Tsukuba, Ibaraki 305*

(Received January 27, 1992; accepted for publication September 19, 1992)

An undoped floating zone (FZ) silicon crystal has been investigated by synchrotron X-radiation section topography with high-order reflections up to 14 14 0. Numerically simulated topographs based on the Takagi-Taupin equations were in good agreement with experimental distorted patterns when a spherical strain field was assumed in the crystal. The volume change of the lattice caused by the strain center was estimated to correspond to a sphere with a radius of 10 μm.

KEYWORDS: synchrotron radiation, X-ray diffraction, dynamical scattering, high-order reflection, topography, silicon, strain center, microdefect, Takagi-Taupin equations, computer simulation

§1. Introduction

Recently, increasing integrations of electronic devices on silicon wafers have given rise to growing demands for the characterization of microdefects in silicon crystals.

In previous papers of the Toyama University group,[1-3] the authors reported the Pendellosung fringe method by X-ray section topography for characterizing oxygen-induced microdefects in heat-treated Czochralski-grown (CZ) silicon crystals. In the cases of refs. 1-3, since microdefects were distributed with very high density (10^7–10^{13}/cm^3) and sizes of defects were very small (several hundreds to one thousand ångströms),individual defects were not detectable with topographic resolution while strain fields elongating spacings of Pendellösung fringes could be dealt with statistically.[4,5] In ref. 3, the authors reported the synchrotron X-radiation section topography with high-order reflections improving the accuracy of the Pendellösung fringe method. It was also pointed out that high-order reflection section topography was effective for detecting very faint strain fields which irregularly disturbed Pendellösung fringes. Such faint strain fields could not be detected by the conventional section topography with low-order reflections. The present paper gives an example of such distorted topograph patterns interpreted with a simple model of strain field caused by a single microdefect.

For detecting individual microdefects in silicon crystals, several special techniques of X-ray topography have been reported. Chikawa *et al.*[6] introduced the weak beam method in X-ray topography. They successfully observed microdefects in an as-grown floating zone (FZ) silicon crystal with reduced background of dynamical diffraction by the kinematical image technique (KIT). KIT lead Renninger[7] to the idea of plane-wave topography with off-Bragg weak beam conditions, and lead Köhler *et al.*[8] to the gap topograph technique. Renninger and Köhler *et al.* also successfully observed microdefects in as-grown FZ-silicon crystals. Chikaura *et al.*[9] applied the plane-wave topography to a CZ-silicon crystal thinned to a thickness near the extinction distance. Ishikawa[10] developed the ultra-plane wave topography using the synchrotron radiation, by which fine concentric circular images caused by microdefects were observed. Kawado *et al.*,[11] also by the ultra-plane wave topography, observed microdefects as dot images in magnetic-field-applied Czochralski-grown (MCZ) silicon crystals. The experimental technique used in the present work was intended simply to use high-order reflections in X-ray section topography, which gives a relatively simple and effective method with the use of synchrotron radiation.

In order to evaluate the observed strain field, the present authors used the simulation method in which the Takagi-Taupin equations[12-15] were numerically integrated. The first study in which a numerically simulated section topograph was compared with an experimental one has been performed by Balibar and Authier, for a crystal containing a dislocation.[16] Later, this simulation method and its applications were investigated in detail by Epelboin.[17,18]

Although study on strain centers (or pointlike defects) by the simulation method have long been not published to the present authors' knowledge, recently, Green *et al.*[19] reported a study on strain centers using the simulation method. Whereas they investigated the case in which strain centers existed inside the Borrmann fan, in the case of the present work, a strain center was assumed to exist outside the Borrmann fan and the magnitude of the strain field (the proportional constant c in eq. (6)) was estimated to be about 10^4 times greater than those reported by Green *et al.*

*Present address: Isobe R&D Center, Shin-Etsu Handotai Co., Ltd., Isobe, Annaka, Gumma 379-01.
**Present address: LSI Research and Development Laboratory, Mitsubishi Electric Corporation, Itami, Hyogo 664.

§2. Experimental

The sample used in the X-ray diffraction topography was a (111)-oriented wafer of as-grown dislocation-free silicon crystal of high purity, which had been grown in the [111] direction by the floating zone method. The resistivity of the sample was about 70 Ω·cm. Impurity concentrations were measured by Fourier transform infrared absorption spectroscopy, and estimated to be less than the detection limit (5×10^{15} atom·cm^{-3}) for oxygen and about 7×10^{15} atom·cm^{-3} for carbon. The dimensions of the sample wafer with egg-shaped contours were 36 mm × 32 mm. The surfaces of the sample wafer were prepared by mechano-chemical etching to remove the damaged layers induced in the cut-off process from the ingot. The thickness of the sample was 3.30 mm.

The topographic observation was carried out at the National Laboratory for High Energy Physics, using Beam Line 15B of the Photon Factory. Figure 1 shows the experimental arrangement for the X-ray diffraction topography. The polarization of X-rays of Beam Line 15B was horizontal, and the optical system was arranged so that the directions of the incident and reflected beams lay on a vertical plane. Therefore the electric polarization vectors of the beams were normal to the sheet in Fig. 1.

The synchrotron white radiation was monochromatized with a silicon (111) asymmetrical monochromator. The beam reflected by the monochromator was tuned into a wavelength of 0.4 Å. The asymmetrical factor of the monochromator was 14, so that the beam incident on the monochromator with a high angle was reflected with a low take-off angle to be condensed into a narrow beam. The angular divergence of the beam from the monochromator was calculated to be 3.1×10^{-5} rad with the wavelength being constant, based on the dynamical theory. The monochromatized beam passed through an ion chamber of argon gas, with which the intensity of the beam was monitored. Then the beam whose width was limited by a slit was incident on the sample crystal. Reflections 8 8 0, 12 12 0 and 14 14 0 were searched with a scintillation counter. Since the rotating axis of the goniometer on which the sample was set, lay on the incident surface of the sample wafer, the positions of the apexes of the Borrmann fans were identical for these reflections (see Fig. 6). The intensity of the wave reflected by the sample crystal in the symmetrical Laue geometry, was recorded on nuclear plates with 50 μm emulsion thickness.

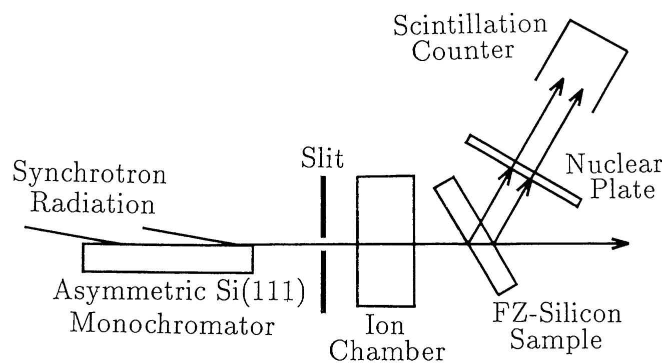

Fig. 1. The experimental arrangement of the X-ray section topography using the synchrotron radiation. The electric polarization vectors of the incident and reflected beams were normal to the sheet.

Table I shows parameters characterizing the reflections whose indices of scattering vectors $\boldsymbol{h}$ are 8 8 0, 12 12 0 and 14 14 0, where θ_B is the Bragg-reflection angle, χ_{+h} and χ_{-h} are the plus and minus $\boldsymbol{h}$-th Fourier coefficients of the electric polarizability, ω_s is the angular width of the Bragg-reflection, and τ is the extinction distance. The expressions of ω_s and τ are given by

$$\omega_s=\frac{2C|\chi_h|}{\sin 2\theta_B}, \quad (1)$$

$$\tau=\frac{\cos\theta_B}{KC|\chi_h|}, \quad (2)$$

where K is the wave number of the incident wave which is equal to 2.5×10^{10} m^{-1} for the wavelength of 0.4 Å, and C is the polarization factor which is equal to unity in the present case.

Each ω_s is sufficiently small compared with the angular divergence of the incident beam, whose value is 3.1×10^{-5} rad as described above. Hence, the experimental condition for each reflection was regarded as the case of an incident spherical wave.

Table II shows the type of nuclear plate, slit width, exposure time and ring current of the Photon Factory storage ring during exposure for each reflection in the present experiment.

Table II. Experimental conditions in which the section topographs shown in Fig. 4 were taken.

Reflection index	Type of nuclear plate	Slit width (μm)	Exposure time (hours)	Storage ring current (mA)
8 8 0	Ilford L4	50	2.9	128
12 12 0	Ilford G5	100	6.4	175
14 14 0	Ilford G5	100	12.3	221

Table I. Several parameters characterizing each reflection of silicon whose vector $\boldsymbol{h}$ is 8 8 0, 12 12 0 or 14 14 0, for 0.4 Å wavelength at room temperature. θ_B is the Bragg-reflection angle, χ_{+h} and χ_{-h} are the plus and minus $\boldsymbol{h}$-th Fourier components of the electric poralizability, ω_s is the angular width of the Bragg-reflection, τ is the extinction distance.

Reflection index	θ_B (deg)	$\sqrt{\chi_{+h}\chi_{-h}}$ Real	Imaginary	ω_s (rad)	τ (m)
8 8 0	24.62	1.11×10^{-7}	9.09×10^{-10}	2.93×10^{-7}	3.28×10^{-4}
12 12 0	38.68	3.54×10^{-8}	4.84×10^{-10}	7.26×10^{-8}	8.82×10^{-4}
14 14 0	46.81	2.09×10^{-8}	3.21×10^{-10}	4.19×10^{-8}	1.31×10^{-3}

§3. Simulation

The Takagi-Taupin equations[12-15] (the T-T equations) are the fundamental equations of the theory of X-ray dynamical scattering, which are applicable to the diffraction in a distorted crystal with an arbitrary incident wave condition. In the simulations of the present work, the authors adopted the following type T-T equations with good symmetry, which were presented by Kato:[15]

$$\frac{\partial D_o}{\partial s_o}=AD_h, \quad (3.a)$$

$$\frac{\partial D_h}{\partial s_h}=BD_o, \quad (3.b)$$

where A and B are given by

$$A=-\mathrm{i}\pi KC\chi_{-h}\exp(-2\pi\mathrm{i}\boldsymbol{h}\cdot\boldsymbol{u}), \quad (4.a)$$

$$B=-\mathrm{i}\pi KC\chi_{+h}\exp(+2\pi\mathrm{i}\boldsymbol{h}\cdot\boldsymbol{u}), \quad (4.b)$$

Here, D_o and D_h are the amplitudes of refracted and reflected waves, s_o and s_h are the oblique coordinates in the direction of refraction and reflection, K is the wave number of the incident wave, C is the polarization factor, $\boldsymbol{h}$ is the reflection vector, χ_{+h} and χ_{-h} are the plus and minus $\boldsymbol{h}$-th Fourier coefficients of the electric polarizability and $\boldsymbol{u}$ is the lattice displacement vector.

One can obtain wave fields in the crystal with arbitrary strain field by solving eqs. (3.a) and (3.b) under the boundary condition appropriate for the incident wave packet. The basic principle for solving the T-T equations in the present work was the same as that described by Epelboin in his reviews.[17,18] In order to integrate the T-T equations, the plane of incidence, which is parallel to the directions of both refraction and reflection, was covered with fine meshes as shown in Fig. 2. Figure 3 shows a piece of the wedge cut off by a mesh in Fig. 2. The amplitudes of the refracted and reflected waves at the point R are obtained from those at the points P and Q by solving the following difference equations:

$$\frac{x-c}{l}=A\frac{d+y}{2}, \quad (5.a)$$

$$\frac{y-b}{l}=B\frac{a+x}{2}, \quad (5.b)$$

where A and B are given by eqs. (4.a) and (4.b), and the other parameters are as shown in Fig. 3; that is, a, b, c, d and x, y are the amplitudes of refracted and reflected waves at the points P, Q and R, and l is the length of PR which is equal to QR. The length l must be sufficiently small compared with the extinction distance τ which roughly gives the periodic length of Pendellösung oscillation of X-rays in the crystal.

When a boundary condition is given, the difference equations (5) can be solved. That is, the amplitudes of the refracted and reflected waves in the crystal can be calculated step by step from the amplitudes of the wave incident on the crystal surface. In the experiments of the present work, the condition of spherical wave incidence was satisfied as described in §2. This condition is equivalent to the situation where the amplitude of the incident wave packet is localized in a sufficiently small region on the crystal surface compared with the extinction distance τ of each reflection. Therefore, for the

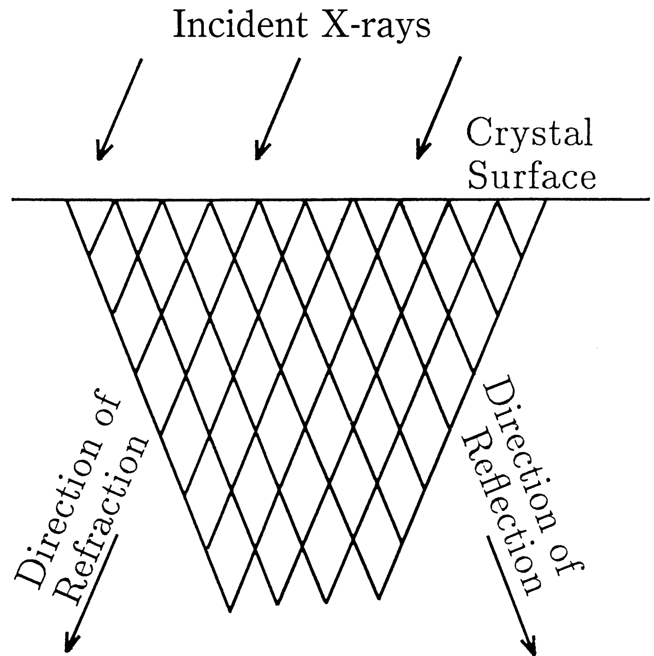

Fig. 2. A plane of incidence in the crystal was covered with fine meshes. One can numerically integrate the difference forms of the T-T equations (eqs. (5.a) and (5.b)) step by step toward the exit surface of the crystal from the incident surface where the boundary condition is given.

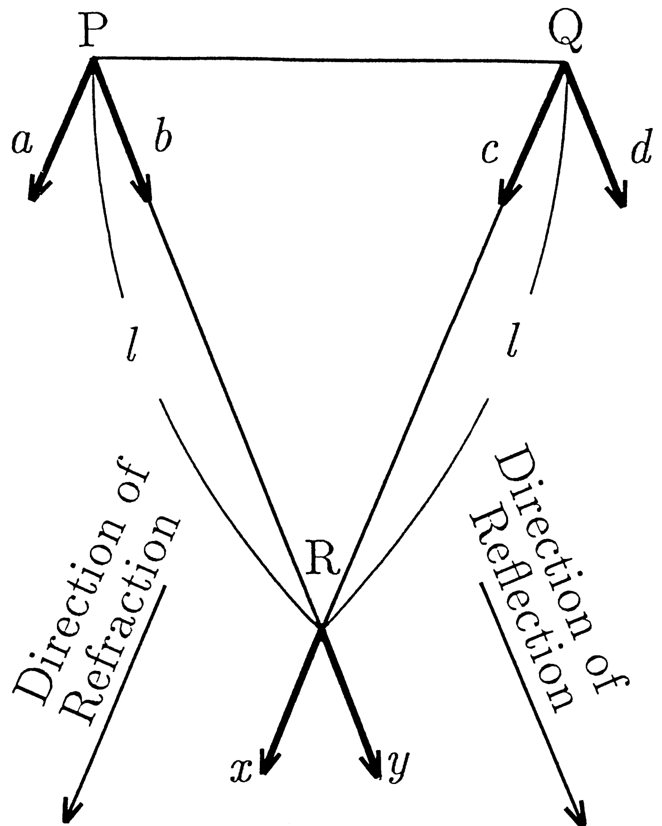

Fig. 3. One small wedge cut off from Fig. 2, where a, b, c, d and x, y are the amplitudes of refracted and reflected waves at the points P, Q and R respectively.

boundary condition of the incident spherical wave, at only one point on the incident surface of the crystal, a value not equal to zero was given for the amplitude of the refracted wave.

To solve eqs. (5), the lattice displacement $\boldsymbol{u}$ in the crystal is necessary because the parameters A and B depend on $\boldsymbol{u}$. The present authors assumed that the strain field was induced by a single strain center in an isotropic elastic continuum. Then, the lattice displacement vector $\boldsymbol{u}$ was assumed to be given by

$$u=\frac{c}{r^2}\hat{r}, \tag{6}$$

where c is the magnitude of the strain field, r is the distance from the strain center, and $\hat{r}$ is the unit vector of the direction of r.

When the spherical strain field was assumed in the simulation to be compared with the experimental patterns, there were three adjustable parameters, that is, horizontal and vertical coordinates of the strain center (see Fig. 6), and the magnitude of the strain field c in eq. (6). The calculations were executed in 500 steps in the depth direction of the crystal, which divides the crystal into sufficiently small wedges compared with the extinction distance τ. The above calculation was repeated from one plane of incidence to another in the direction of the height of the beam (normal to the sheet in Fig. 6); then, a two dimensional pattern was obtained. Until the patterns best fitted to the experimental results were obtained, the simulation was repeated over and over again. FACOM-M360 and IBM-3081 mainframe computers of Toyama University and NEC-PC9801VX21 personal computer were used for the calculations. One trial of the simulation took about 20 min of central processing unit (CPU) time on the mainframe computers and about 20 h on the personal computer. Calculated intensities of reflected waves were displayed on the cathode ray tube of the NEC-PC9801VX21 personal computer with 16 degrees of brightness and were photographed on Fuji Neopan SS film.

§4. Results and Discussion

The experimental section topographs were obtained as shown in Fig. 4. One can observe disturbances in the lower parts and upper parts of Fig. 4. The present authors regarded disturbances of the lower parts as caused by the wax used to mount the sample crystal. The simulations of the present work were concerned with the disturbed patterns in the upper regions of the topographs in Fig. 4. As for 14 14 0 reflection, in Fig. 4(a) one can observe 4-fold concentric circles and a white band diagonally crossing the concentric circular pattern. As for 12 12 0 reflection, in Fig. 4(b) one can observe a 2-fold elliptical spot. As for 8 8 0 reflection, in Fig. 4(c) one can observe the Pendellösung fringe of the center which is slightly swelled in the upper region.

Figure 5 shows the best fitted simulation patterns together with the experimental patterns magnified from the upper parts of Fig. 4. When the magnitude of the strain field (the proportional constant c in eq. (6)) was $\pm 4\times 10^{-16}$ m^3, the simulation patterns best fitted the experimental ones. Figure 6 shows the location of the strain center determined by the simulation.

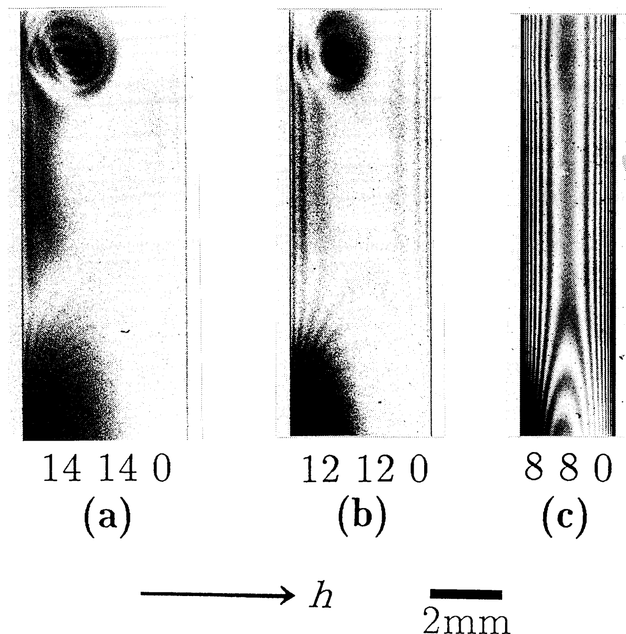

Fig. 4. The experimental section topograph patterns for (a) 14 14 0, (b) 12 12 0 and (c) 8 8 0 reflection. The simulations of the present work were concerned with the disturbed patterns in the upper regions.

As for 14 14 0 reflection, in the simulation patterns Figs. 5(a) and 5(c), 4-fold concentric circles and a white band similar to the experimental pattern Fig. 5(b), were observed. The correspondence was excellent. The present authors regarded the tilt of the white band in the experimental pattern Fig. 5(b) as caused by the strain field disturbing the lower parts of Fig. 4. As for 12 12 0 reflection, in the simulation patterns Figs. 5(d) and 5(f), an elliptical spot was observed. The ratio of the height of the spot to the width was similar to that of the experimental pattern Fig. 5(e). The 2-fold elliptical pattern was, however, not simulated. As for 8 8 0 reflection, in Figs. 5(g) and 5(i), the Pendellösung fringe of the center was swelled slightly as found in the experimental pattern Fig. 5(h).

Comparing the topographs of 8 8 0 reflection which was not significantly distorted, with the topographs of 12 12 0 and 14 14 0 reflections, one can see the great advantage of higher-order reflection in detecting strain field in the sample crystal.

Figure 5 shows the simulation patterns for the strain field of both positive and negative magnitude. Although the simulated results for positive and negative magnitude of the strain field were slightly different owing to the absorption of X-rays in the crystal, the difference was too small to determine the sign of the magnitude of the strain field. Thus, it could not be determined whether the strain center expanded or contracted the surrounding lattice.

The volume change of the lattice caused by the strain center could be estimated to be the volume of a spherical shell whose thickness is $u(=cr^{-2})$ and radius is r, that is, estimated at $4\pi c$ corresponding to the volume of a sphere

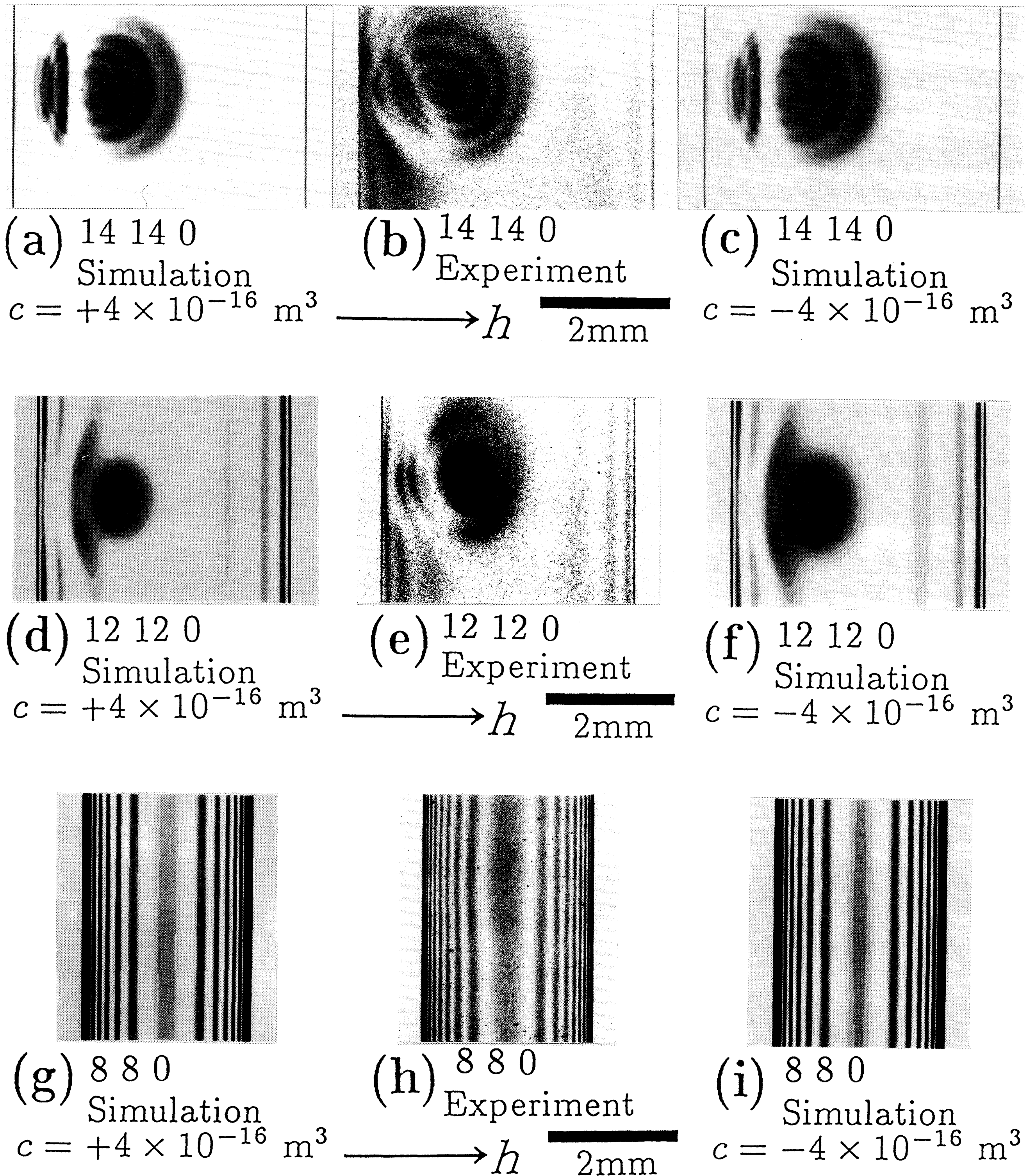

Fig. 5. The comparison between the experimental and the numerically simulated section topographs. The value of c indicates the magnitude of the strain field in eq. (6).

with a radius of about 10 μm.

In order to estimate the accuracy of the above evaluation, the simulation where the magnitude of the strain field was slightly changed from the best fitted value 4×10^{-16} m^3, was carried out. Figure 7 shows the results of the simulation for 14 14 0 reflection, where the magnitude of the strain field (the proportional constant c in eq. (6)) was -3×10^{-16} m^3 for Fig. 7(a), and -5×10^{-16} m^3 for Fig. 7(b). The strain center was located at the same position as that for the best fitted simulation as shown in Fig. 6. One can observe 3-fold concentric circles in Fig. 7(a) and 5-fold concentric circles in Fig. 7(b), which were significantly different from the experimental pattern Fig. 5(b) and the best fitted simulation patterns Figs. 5(a) and 5(c) where 4-fold concentric circles were observed. Then one can see the degree of ac-

curacy in estimating the magnitude of the strain field in this simulation method.

Although in the present work the simulation was executed on the assumption of a spherically symmetrical strain field, the actual strain field caused by a single strain center is not strictly spherically symmetrical owing to the stress relaxation on the crystal surfaces. For more precise analysis of the strain field, it is necessary to correct the spherical strain field with the image forces.

In order to characterize the strain center itself, several investigations are in progress. It is, however, still unclear what induced such a big strain field.

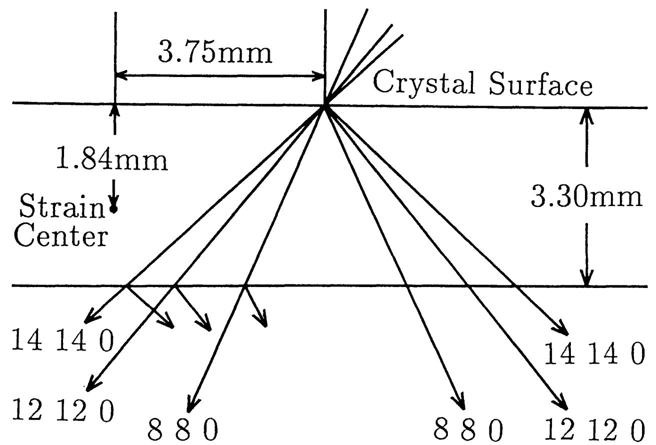

Fig. 6. The location of the strain center which was determined by the comparison between the experiment and the simulation.

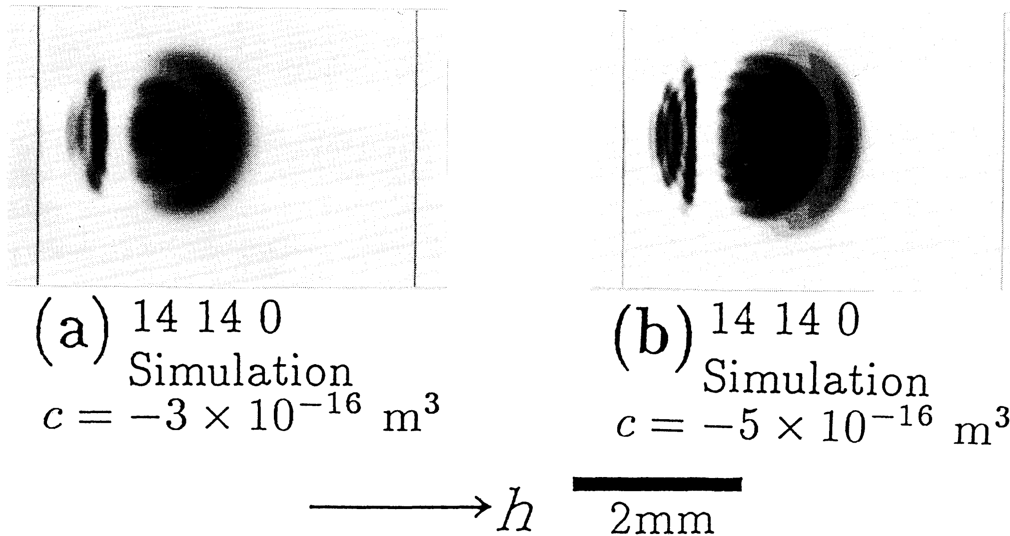

Fig. 7. Numerically simulated section topograph images of the spherical strain field whose magnitude (the value c in eq. (6)) was slightly changed. These patterns were significantly different from the best fitted simulation (Fig. 5(c)) where the magnitude of the strain field was -4×10^{-16} m^3.

§5. Conclusions

Distorted patterns were observed in section topographs of a high-purity FZ-silicon crystal. The present authors could detect the strain field owing to the following two advantages of the synchrotron radiation section topography over the conventional section topography. First, a thick (3.3 mm) sample crystal could be used owing to less absorption of the short (0.4 Å) wavelength X-rays in the crystal. The use of the thick crystal enabled the present authors to obtain the information on lattice strain from a large region of the crystal at one trial of exposure. Secondly, the high-order reflections (up to 14 14 0) with low scattering powers could be used owing to the high intensity of the synchrotron radiation. The higher the order of Bragg-reflection is, the greater is the sensitivity of the section topograph pattern to the lattice strain.

In addition, the distorted patterns observed were well reproduced in the simulations based on the Takagi-Taupin equations where a spherical strain field was assumed in the crystal. The strain field was estimated to cause a volume change in the lattice corresponding to a sphere with a radius of about 10 μm.

Acknowledgments

The authors are indebted to Dr. T. Abe of Shin-Etsu Handotai for providing the FZ-silicon crystal. This work has been performed under the approval of the Photon Factory Program Advisory Committee (Proposal No. 86-152).

References

1) Y. Sugita, H. Sugiyama, S. Iida and H. Kawata: Jpn. J. Appl. Phys. **26** (1987) 1903.
2) S. Iida, H. Sugiyama, Y. Sugita and H. Kawata: Jpn. J. Appl. Phys. **27** (1988) 1081.
3) S. Iida, H. Takeno, Y. Sugita and H. Kawata: Jpn. J. Appl. Phys. **29** (1990) 970.
4) N. Kato: Acta Crystallogr. A **36** (1980) 763.
5) N. Kato: Acta Crystallogr. A **36** (1980) 770.

6) J. Chikawa, Y. Asaeda and I. Fujimoto: J. Appl. Phys. **41** (1970) 1922.
7) M. Renninger: J. Appl. Crystallogr. **9** (1976) 178.
8) R. Köhler, W. Möhling and M. Pasemann: Phys. Status Solidi **53** (1979) 509.
9) Y. Chikaura, M. Imai and T. Ishikawa: Jpn. J. Appl. Phys. **26** (1987) L889.
10) T. Ishikawa: Rev. Sci. Instrum. **60** (1989) 2490.
11) S. Kawado, S. Kojima, Y. Kato, H. Hayashi and T. Ishikawa: *Defect Control in Semiconductors*, ed. K. Sumino (Elsevier, Amsterdam, 1990) p. 175.
12) S. Takagi: Acta Crystallogr. **15** (1962) 1311.
13) S. Takagi: J. Phys. Soc. Jpn. **26** (1969) 1239.
14) D. Taupin: Bull. Soc. Fr. Mineral & Cristallogr. **87** (1964) 469.
15) N. Kato: Z. Naturforsch. a **28** (1973) 604.
16) F. Balibar and A. Authier: Phys. Status Solidi **21** (1967) 413.
17) Y. Epelboin: Mater. Sci. Eng. **73** (1985) 1.
18) Y. Epelboin: Prog. Cryst. Growth & Charact. **14** (1987) 465.
19) G. S. Green, Cui Shu Fan and B. K. Tanner: Philos. Mag. A **61** (1990) 23.